Tetrahedron 72 (2016) 7357–7373

Contents lists available at ScienceDirect

Tetrahedron

journal homepage: www.elsevier.com/locate/tet

Tetrahedron report 1128

Thermally activated tunneling in organic reactions

Edyta M. Greer [a,*], Kitae Kwon [a], Alexander Greer [b], Charles Doubleday [c]

[a] Department of Natural Sciences, Baruch College of the City University of New York, 17 Lexington Avenue, New York, NY 10010, United States
[b] Department of Chemistry and Graduate Center, Brooklyn College of the City University of New York, 2900 Bedford Avenue, Brooklyn, NY 11210, United States
[c] Department of Chemistry, Columbia University, 3000 Broadway, MC 3142, New York, NY 10027, United States

ARTICLE INFO

Article history:
Received 10 August 2016
Available online 16 September 2016

Contents

* Corresponding author. E-mail address: edyta.greer@baruch.cuny.edu (E.M. Greer).

http://dx.doi.org/10.1016/j.tet.2016.09.029
0040-4020/© 2016 Elsevier Ltd. All rights reserved.

1. Introduction

Tunneling through a barrier[1] is a consequence of the wave nature of matter. If the thickness of the barrier is approximately equal to or less than the de Broglie wavelength of a particle approaching the barrier, then tunneling can occur. Tunneling increases the rate of a chemical reaction because it occurs *in addition* to passage over the barrier. Since it accesses lower energy pathways for reaction, it can lower the measured activation energy. The degree to which that occurs depends on the shape of the barrier, the atomic masses, and the temperature; the role of each will be discussed below. Thermally activated tunneling[2] means that most of the tunneling contribution to the rate comes from excited vibrational levels of the reactant, as opposed to the zero-point level, ν=0 (Fig. 1). In many reactions in which tunneling is important, tunneling from ν=0 is negligible. In Section 3 we discuss the effect of barrier shape, atomic mass and temperature on tunneling probabilities and rates of reactions.

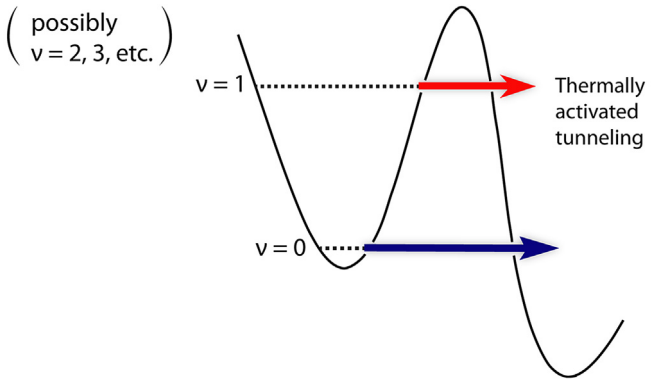

Fig. 1. Thermally activated tunneling (ν=1) or higher excited vibrational levels (ν=2, 3, etc.) and tunneling from the lowest vibrational level (ν=0).

2. Scope

This review is meant to be of interest to organic chemists. Literature reviews have covered thermally activated tunneling,[3–5] theoretical treatments of tunneling,[1,6–8] or were focused on tunneling in materials[1,9] and enzymes.[7,10–17] Tunneling at cryogenic temperatures (e.g., Argon matrix at 10 K) has also been reviewed before[1,3–5,18–20] where low thermal energy halts the reaction from proceeding over the barrier, but we deem such examples to be outside the norm of bench top organic reactions.

No reviews exist that target tunneling at temperatures commonly encountered in organic chemistry, which is done here. In Section 3, a background on tunneling is provided. The remainder of the review has been divided into two sections describing the tunneling of carbon or nitrogen, and hydrogen, which cover literature over the past ~10 years (Sections 4 and 5). In Section 4, carbon- and nitrogen-atom tunneling is described (Fig. 2). In Section 5, literature is covered on H-atom transfer, and H^- and H^+ transfer reactions in organic chemistry (Fig. 2). Useful aspects of experimental and computational methods for evidence of tunneling in organic chemistry are also included.

3. Background

A particle approaching a parabolic barrier is a good qualitative model for tunneling. If the particle has mass m and energy E, and the barrier has height V and width w, the tunneling probability is proportional to $\exp(-w[m(V-E)]^{1/2})$. The barrier width has the greatest effect on tunneling because it occurs as the first power. The mass dependence is not as strong, but clearly is important for kinetic isotope effects (KIEs).

In transition state theory (TST), the effect of tunneling on the rate constant k is contained in the transmission coefficient κ, i.e., $k=\kappa(k_BT/h)\exp(-\Delta G^{\ddagger}/RT)$. κ is the quantum correction for motion along the reaction coordinate. It includes the effect of forward transmission through the barrier and backward reflection (diffraction) above it. With this definition, κ is the ratio of the tunneling-corrected rate to the classical rate (TST); κ=1 if there is no tunneling and κ>1 if tunneling contributes to the rate. We take $(\kappa-1)/\kappa$ as a convenient measure of the fraction of reaction due to tunneling (actually a lower bound, because κ is tunneling minus reflection), so that κ=2 implies 50% tunneling.

The clearest experimental evidence for tunneling has been obtained at cryogenic temperature.[1,3–5,18–20] With negligible thermal energy, any product formation must be due to tunneling, and the reaction rate is independent of temperature in this regime. As temperature is increased, the fraction of reaction occurring over the barrier increases rapidly. In a hypothetical reaction examined from near 0 K to high temperature, an Arrhenius plot of ln k vs $1/T$ would be straight at high temperature, horizontal at low temperature, and curved in between as shown in the red line in Fig. 3A and C. In contrast, a TST calculation neglecting tunneling would predict a nearly straight line (black). Fig. 3B and D shows an Arrhenius plot of ln(KIE) versus 1/T, where KIE=k_H/k_D (H is hydrogen, D is deuterium) or k^{12}_C/k^{13}_C or k^{14}_N/k^{15}_N, in which an upward curve for tunneling is contrasted to a straight line where there is no tunneling. Common experimental methods used are ^{1}H and ^{13}C NMR, UV/visible and IR spectroscopy.

POLYRATE[21] is a commonly used computational package for computing rates of reaction based on TST with optional inclusion of tunneling. The TST option usually chosen is canonical variational transition state theory, or CVT. The tunneling treatment is typically the small curvature tunneling (SCT) approximation.[22–26]

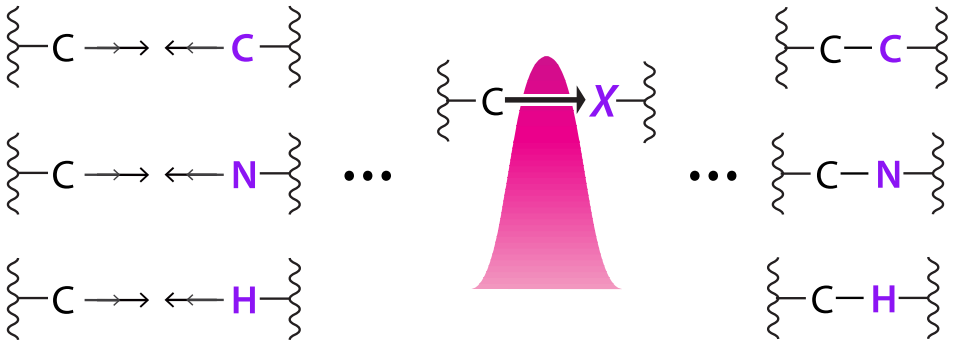

Fig. 2. Schematic illustration of tunneling in carbon–carbon and carbon–nitrogen bond formations, and hydrogen-atom transfer.

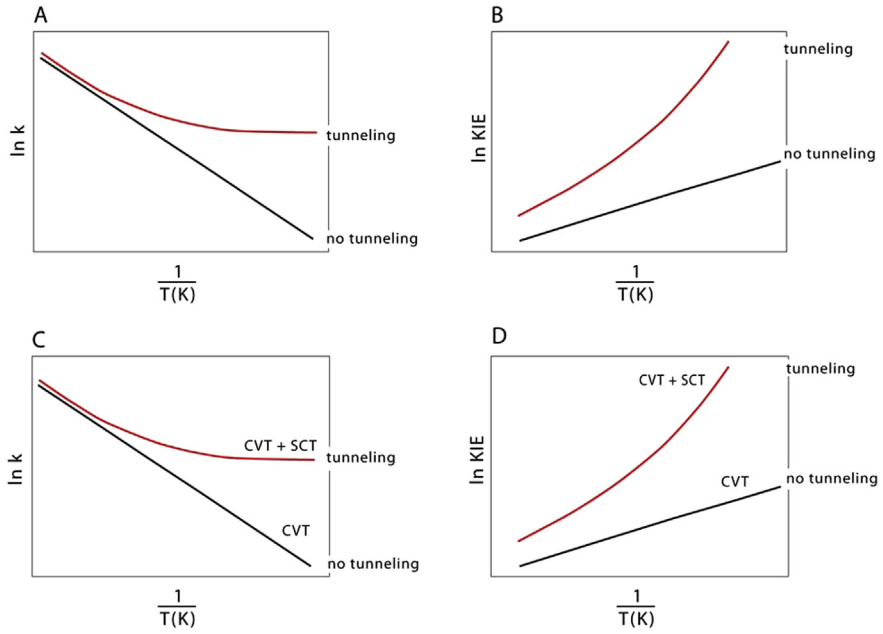

Fig. 3. Experimental Arrhenius plots with ln k (**A**) and ln KIE (**B**). Calculated Arrhenius plots without (CVT) and with (CVT+SCT) the inclusion of tunneling for ln k (**C**) and ln KIE (**D**).

In SCT, *curvature* refers to curvature along the minimum energy path (MEP), which occurs as the path changes direction during the course of a reaction. Regions of high curvature on the MEP create an opportunity for a tunneling particle to 'cut the corner' and tunnel through a shorter distance than the MEP arc length distance. *Small curvature* means that the tunneling path does not stray far from the MEP. Rate constants computed with and without SCT tunneling are $k_{CVT+SCT}$ and k_{CVT}.

In the high-temperature linear portion of a curved Arrhenius plot, tunneling may account for a substantial fraction of the rate. This is the temperature regime where some of the reactions discussed in this review take place. If curvature is not apparent, other tunneling criteria are considered, such as anomalous negative activation entropies (e.g., $\Delta S^{\ddagger} = \sim -10$ to -40 eu),[27] and very large KIEs.[28] For H atom tunneling, the criteria suggested by Kim and Kreevoy[29] are often applied: (a) $k_H/k_D > 7$ at 25 °C; (b) Arrhenius pre-exponential ratio $A_H/A_D < 1.0$; (c) $E_a(D) - E_a(H) > 1.2$ kcal/mol.

Fig. 4 illustrates some features of the dependence of κ on barrier shape and temperature by considering the limiting cases of small versus large barriers. (Numerical values for small vs large depend on the effective tunneling mass.) The shading qualitatively indicates energy regions that contribute to κ over the temperature range of a typical Arrhenius plot. In the small barrier limit, a large temperature range is often accessible. Tunneling can contribute at any energy including the $v=0$ level; the curved region of the Arrhenius plot can be observed, and κ can be very large. For a large barrier, tunneling probabilities may span 30–40 orders of magnitude from the TS down to $v=0$. The range of energies with significant contributions to κ is typically a few times RT below the TS, where the barrier is narrow. As a result, the low temperature curved region of the Arrhenius plot is not observable because the reaction rate becomes too slow. This is particularly true in heavy-atom tunneling with large barriers where the low-energy tunneling probabilities are extremely small.

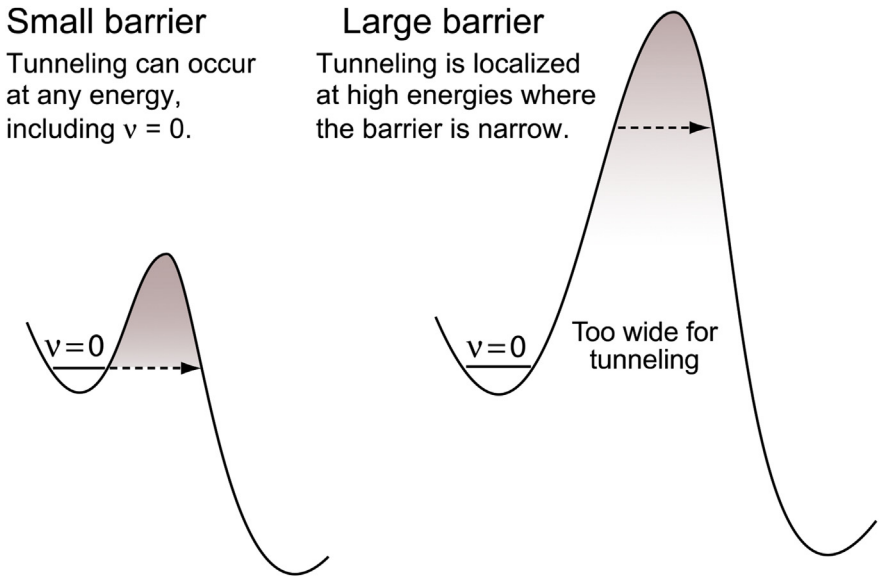

Fig. 4. Tunneling through small versus large barriers. Shaded areas identify regions with substantial contributions to κ. For a given barrier, these regions depend on the tunneling mass and temperature. The shading qualitatively indicates contributions to κ over the temperature range of a typical Arrhenius plot for each barrier.

4. Carbon atom and nitrogen atom tunneling

The examples presented here describe carbon and nitrogen atom tunneling. There are 8 literature examples of which 4 contain both experimental *and* theoretical evidence, and 3 that contain theoretical evidence alone.

4.1. Ring-opening of a cyclopropylcarbinyl radical

A 2010 report describes the ring-opening of cyclopropylcarbinyl radical **1** where experimental and computational studies provided evidence for carbon atom tunneling (Scheme 1).[30] To reach **1**, (bromomethyl)cyclopropane was reacted with $Bu_3Sn^{\bullet}$. An additional step with Bu_3SnH afforded 1-butene and methylcyclopropane.

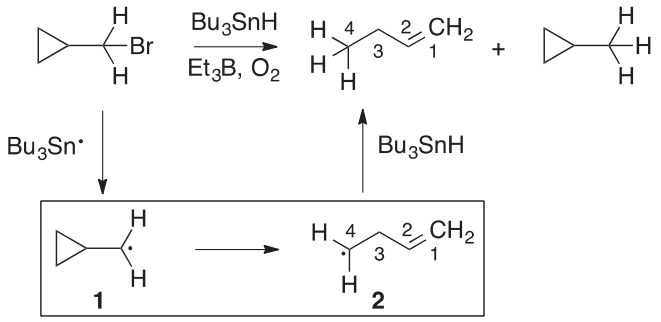

Scheme 1. (Bromomethyl)cyclopropane reaction leading to the ring opening of the cyclocyclopropylcarbinyl radical **1**. Carbon atom numbering is shown.

A stated goal of this study[30] was to obtain prima facie experimental evidence for tunneling – that is, experimental results that imply tunneling without recourse to calculation. The relative amount of ^{13}C at positions 3 and 4 of 1-butene was analyzed by NMR at natural abundance at five temperatures from −100 to +80 °C. This gave intramolecular KIEs, defined as $[k_{12C}/k_{13C}$ (at C4)]/$[k_{12C}/k_{13C}$ (at C3)], ranging from 1.062 at 80 °C to 1.163 at −100 °C, with uncertainties of ±0.002 to 0.004. Fig. 5 shows the plot of ln (KIE) versus 1/*T*. A linear fit to the experimental data appears acceptable, with R^2=0.99 (this linear fit was not mentioned in ref 30; we have plotted the data.) With the small error bars, however, it is clear that the linear fit is inadequate, and must be rejected in favor of a tunneling model that implies curvature. Such a model was provided by POLYRATE calculations that predicted a curved plot that fit the data. By itself, the experimental plot in Fig. 5 implies tunneling, because the points do not lie on a line and TST demands a linear plot. The high precision of the NMR measurements was critical here.

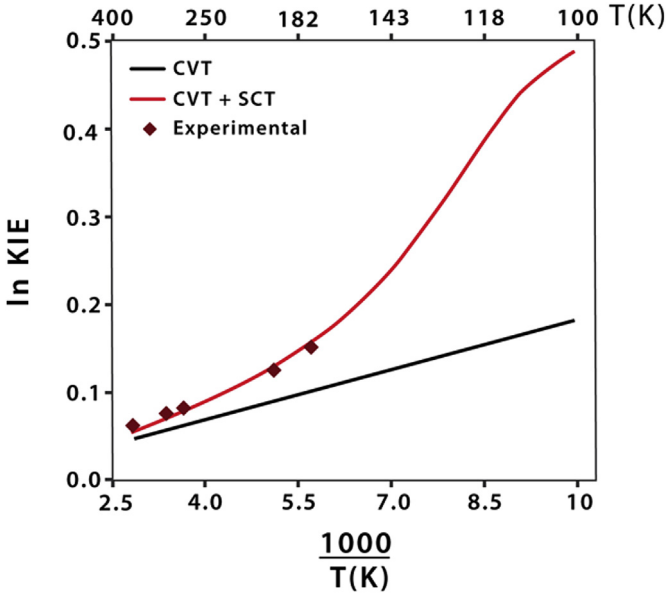

Fig. 5. Experimental and calculated Arrhenius plots for the ring opening of **1** (ln KIE is $[k_{12C}/k_{13C}$ (at C4)]/$[k_{12C}/k_{13C}$ (at C3)]) over the temperature range of 100 K–353 K. The calculations were without (CVT) and with (CVT+SCT) the inclusion of tunneling. Adapted with permission from ref 30. Copyright 2010 American Chemical Society.

Given the nonlinearity, the three highest and the two lowest temperature points were analyzed in separate linear plots. The high-*T* points gave $E_a(^{13}C)-E_a(^{12}C)$=0.052 kcal/mol and A_{12C}/A_{13C}=0.987; the low-*T* points gave $E_a(^{13}C)-E_a(^{12}C)$=0.085 kcal/mol and A_{12C}/A_{13C}=0.908. The large difference in $E_a(^{13}C)-E_a(^{12}C)$ is consistent with tunneling, as is $A_{12C}/A_{13C}<1$. Furthermore, KIE computed by CVT+SCT matched well with the experimental data, but the calculated KIE based on CVT alone (without tunneling) did not.

4.2. The Roush allylboration of aldehydes

A 2012 paper reported experimental and computational $^{12}C/^{13}C$ KIE data at −78 °C for the reaction of anisaldehyde **3** with Roush (+)-diisopropyl L-tartrate-modified allylboronate **4** to reach allylic alcohol **5** (Scheme 2).[31]

Experimental evidence for tunneling included $^{12}C/^{13}C$ KIE values that were larger than 1.00 at C1, C2, and C4 of 1.052, 1.036, and 1.019, respectively, for **3**+**4** reaching **5**. Computational evidence for tunneling included M06-2X/6-31+G(d,p) calculations of $KIE_{CVT+SCT}=k_{12C}/k_{13C}$ and $KIE_{CVT}=k_{12C}/k_{13C}$ were conducted in the gas phase and with polarized continuum model (PCM) of CH_2Cl_2. The KIE_{CVT} without tunneling were lower than those obtained experimentally, and this underestimation was most distinct for C1 and C2, both of which were most involved in the reaction progress. The calculations with inclusion of tunneling were highly valuable by showing a correlation to the experimental KIE data (Table 1). Computational data showed that 36% of this Roush reaction is due to carbon atom tunneling.

4.3. The Bergman cyclization of an enediyne

In 2013, a paper reported on computations of the Bergman cyclization of (3*Z*)-cyclodec-3-en-1,5-diyne **6** (Scheme 3).[32]

mBLYP//CASSCF and CASSCF computational evidence for carbon atom tunneling included (i) Arrhenius plots of the ln KIEs versus T^{-1} with inclusion of tunneling represented by the red lines in Fig. 6. The blue lines were larger than black Arrhenius plots obtained without tunneling and demonstrated more temperature dependence on the right side where the temperatures is lower. It is because the tunneling contributions increase at lower temperatures. The slope obtained with CVT+SCT over the range −23 °C to 70 °C was 2.5 times the CVT slope, and that difference is expected to be experimentally noticeable. (ii) Computed $^{12}C/^{13}C$ KIEs $[k_{12C}/k_{13C}$ (at C10)]/$[k_{12C}/k_{13C}$ (at C1)] for the conversion of **6** to **7** provide mass increases (^{13}C) at C10 versus C1. The $^{12}C/^{13}C$ KIEs were larger with inclusion of tunneling, $KIE_{CVT+SCT}$=1.049, than without tunneling, KIE_{CVT}=1.028 at −23 °C. Temperatures higher than −23 °C show negligible tunneling. (iii) At 37 °C, tunneling was predicted to have a considerable impact on the rate because of transmission coefficient, κ_{SCT}, value of 1.40 or 1.73 (Fig. 7). Due to κ_{SCT} energy regions through which tunneling contributions are the highest were determined. Tunneling contribution was most significant at the upper portion (1.5 kcal/mol) from the top of the barrier with mBLYP//CASSCF and 2.2 kcal/mol with CASSCF (which is where darker maroon color appears in Fig. 7). Computational data showed that 39% of this enediyne reaction is due to carbon atom tunneling.

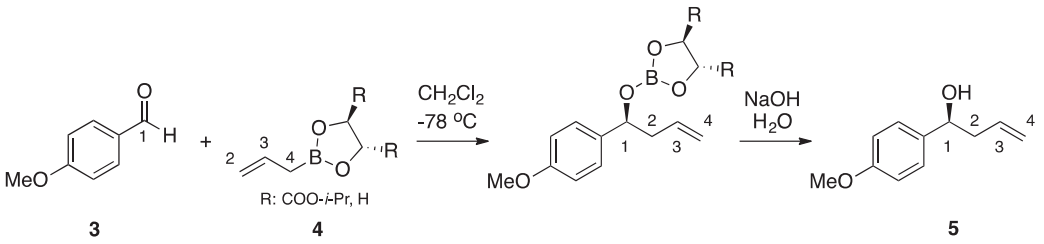

Scheme 2. Reaction of anisaldehyde **3** with allylboronate **4** yielding allylic alcohol **5**. Carbon atom numbering is shown.

Table 1
Computed and experimenta l^{12}C/^{13}C KIEs for the reaction of **3**+**4**

Method	C1	C2	C3	C4
	$KIE_{CVT+SCT}$			
Gas phase	1.047	1.036	0.998	1.020
PCM	1.052	1.038	0.999	1.019
	Experimental KIEs			
	1.052(5)	1.036(5)	0.997(5)	1.019(8)

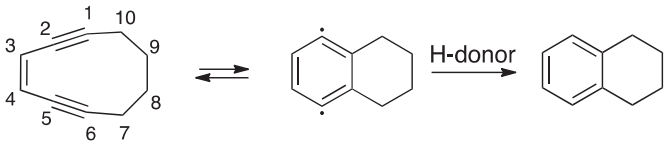

Scheme 3. Bergman cyclization of enediyne **6**.

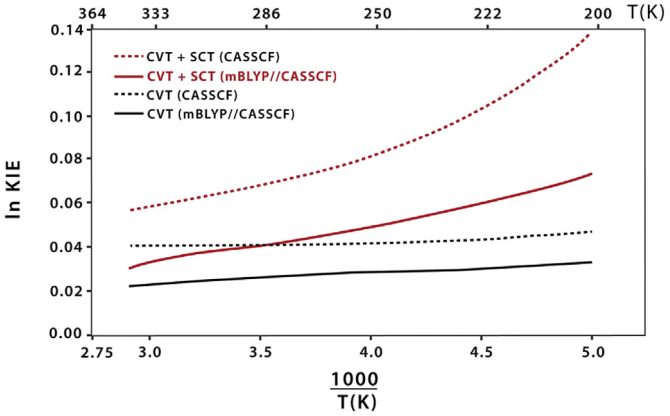

Fig. 6. Arrhenius plot of ln KIE (KIE=[k_{12C}/k_{13C} (at C10)]/[k_{12C}/k_{13C} (at C1)]) versus $1000\times T^{-1}$ computed with mBLYP (solid lines) and CASSCF (dashed lines). Black lines are without (CVT) and red lines are with (CVT+SCT) the inclusion of tunneling. Adapted with permission from ref 32. Copyright 2013 American Chemical Society.

4.4. Myers-Saito cyclization of an annulene

In 2016, a report used computations to examine the Myers-Saito cyclization of cyclodeca-1,2,3,5,9-pentaen-7-yen **9** and ring-fused annulene **12** and found evidence of carbon atom tunneling (Scheme 4).[33]

Computational evidence for tunneling includes: (i) For **9** (Scheme 4A), computations of k_{CVT} was 2.47×10^{-4} s^{-1} and of $k_{CVT+SCT}$ was 3.26×10^{-4} s^{-1}, at 222 K, predicting that the reaction rate is 35 min with tunneling and 45 min without tunneling, of which the former is close to the experimentally measured half-life of 21–31 min. For **12** (Scheme 4B), computations of k_{CVT} was 2.56×10^{-5} s^{-1}, and of $k_{CVT+SCT}$ was 3.36×10^{-5} s^{-1}, at 235 K, predicting that the reaction rate is 5.7 h with tunneling and 7.5 h without tunneling. (ii) ^{12}C3 and ^{12}C2 atoms were substituted with ^{13}C atoms, and primary, secondary, and total (1°+2°) KIEs were obtained for the conversion of **9** to **10**. The primary KIE of **9**→**10** was 1.024 without tunneling, and that with tunneling was 1.099. The secondary KIE_{CVT} of was 1.005 without tunneling, whereas with tunneling it was 1.033. The Arrhenius plot for ln $KIE_{CVT+SCT}$ versus T^{-1} over the temperature range 100 K–300 K was curved suggesting that the tunneling increases the reaction rate. (iii) Without tunneling the E_a^{CVT}=17.1 kcal/mol and log A_{CVT}=13.3 s^{-1}, and with tunneling the $E_a^{CVT+SCT}$=16.8 kcal/mol and log $A_{CVT+SCT}$=13.0 s^{-1} at 222 K, suggesting that the tunneling decreases the energy of activation and thus increases the rate of the Myers-Saito cyclization. (iv) At 200 K, κ_{SCT} values for **9** and **12** were 1.4, and at 298 K both were 1.2, thus indicative of tunneling contribution to the reaction rate. The barrier width for **9** was 1.26 Å, and for **12** was 1.14 Å.

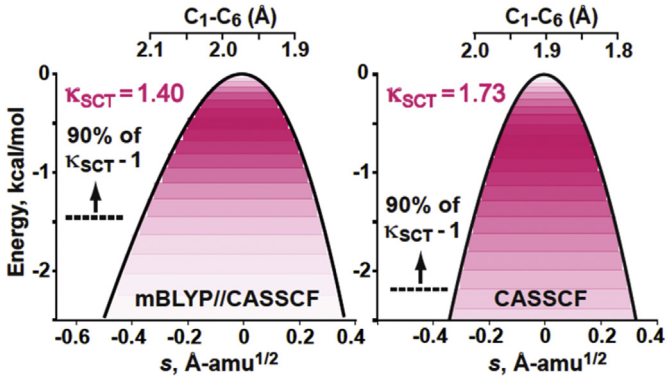

Fig. 7. Tunneling contributions based on mBLYP//CASSCF and CASSCF calculations based on κ_{SCT} for the Bergman cyclization of enediyne **6**. From ref 32. Copyright 2013 American Chemical Society.

4.5. Shifting of the π bonds (automerization) of antiaromatic systems

A historically important report from 1983[34] described the shifting of the π-bonds in cyclobutadiene. This landmark paper was the first unambiguous demonstration of carbon tunneling in a thermal reaction, and it inaugurated the modern study of heavy-atom tunneling. Recently, a computational report from 2014 described the shifting of the π-bonds in pentalene and heptalene via tunneling (Scheme 5).[35]

M06-2X calculations provided evidence for tunneling with an Arrhenius plot of ln $k_{CVT+SCT}$ versus T^{-1} for temperatures of 10 K–400 K. The π-bond shifting of **15** arose because of a narrow barrier width where temperature had little effect on the rate constant. The $k_{CVT+SCT}$ values for **15** were 2.2×10^{8} s^{-1} at 10 K and 7.6×10^{9} s^{-1} at 400 K and are indicative of tunneling. Thus, even at a high temperature of 400 K, automerization of **15** was predicted to proceed by tunneling. Furthermore, computations indicated tunneling contributions in the automerization of π-bonds of a tri-*tert*-butylpentalene **16** and heptalene **17**.[35]

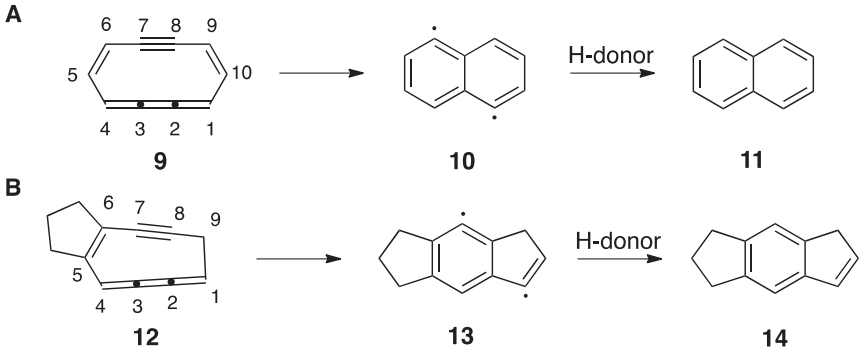

Scheme 4. Myers-Saito cyclization of annulene **9** (**A**) and annulene **12** (**B**).

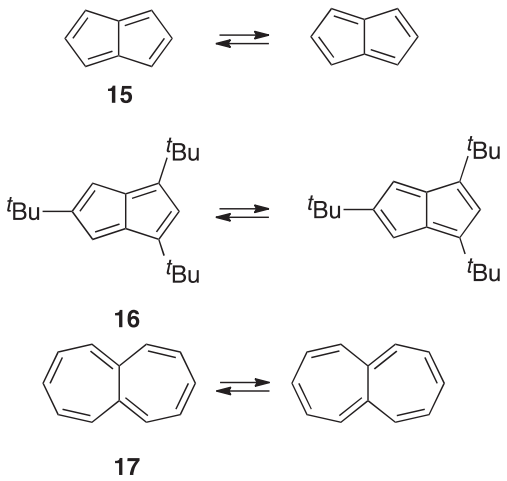

Scheme 5. π-Bond shifting of pentalene **15**, 1,3,5-tri-*tert*-butylpentalene **16**, and heptalene **17**.

4.6. Carbon–carbon bond reductive elimination with gold (III) complexes

Two reports appeared in 2014[36,37] that describe the C–C bond reductive elimination. One report[36] was an experimental study of *cis*-[AuPPh$_3$(4-F-C$_6$H$_4$)$_2$Cl] **18** to form 4,4′-difluorobiphenyl **20** (Scheme 6A), and the other report[37] was a computational study on a model system **21**, which found evidence for carbon atom tunneling (Scheme 6B).

similar electronic properties, energy barriers for reductive elimination of **18** and **21** were similar as well ($\Delta H^{\ddagger}$=17.1 kcal/mol, and 17.5 kcal/mol, respectively). For **21** at −52 °C, k_{CVT} was 5.29×10^{-5} s^{-1}, and with the inclusion of tunneling effect, the $k_{CVT+SCT}$ was 7.43×10^{-5} s^{-1}. The latter value is closer to the experimental rate constant $k_{obs}=1.5\times10^{-4}$ s^{-1} than that of the former. Tunneling was found to occur at 0.14 kcal/mol below the tip of the barrier suggesting that the mode of tunneling is thermally activated. It is also evident from the Arrhenius plot computed with tunneling, which lacks curvature in the range of temperatures from −52 °C to −3 °C. Computations predict that 28% of the C1–C1′ bond formation is due to carbon atom tunneling.

4.7. Linoleic acid oxidation by soybean lipoxygenase 1

In 2011, a paper described the oxidation of linoleic acid **23-*d*$_2$** by soybean lipoxygenase 1 (Scheme 7).[38] First, there was the formation of a pentadienyl radical by hydrogen atom abstraction at C11, which was followed by the addition of dioxygen at C13 and a subsequent H-abstraction step to reach **26-*d***. This reaction involved carbon-atom tunneling through the hydrogen abstraction process via carbon (k_{12C}/k_{13C}) KIE at C11.[38]

Table 2 shows experimental evidence for tunneling included ^{12}C/^{13}C KIEs for linoleic acid **23-*d*$_2$** oxidation by soybean lipoxygenase 1. The ^{12}C/^{13}C KIE for C11 directly involved in the hydrogen abstraction was high compared to C9, C10, C12, and C13. The KIE values are apparently greater than 1,000, although the error bounds are fairly high, which may reflect the difficulty of measurements in a biological sample. B3LYP/6-31+G(d,p) calcu-

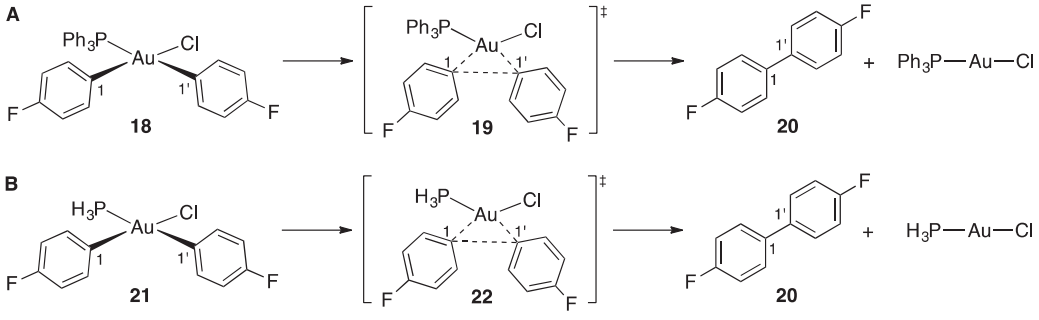

Scheme 6. Reductive elimination of a biphenyl compound from gold(III) complex **18** (**A**) and **21** (**B**).

Experimental data showed that the reaction of Au(III) complex **18** to form 4,4′-difluorobiphenyl **20** and (Ph$_3$P)AuCl was rapid at −52 °C with $k=1.5\pm0.1\times10^{-4}$ s^{-1}. Computational evidence for tunneling included results on **21** as a model system. Since PPh$_3$ and PH$_3$ share similar electronic properties, their energy barriers were

lations provided further evidence for carbon atom tunneling in 2,5-heptadiene-4,4-d_2 as a model for **23-*d*$_2$**. In 2,5-heptadiene-4,4-d_2 the equilibrium isotope effects were calculated. The calculated isotope effects at C4 were in reasonable agreement with the experimental data for **23-*d*$_2$**. This was taken as an evidence of

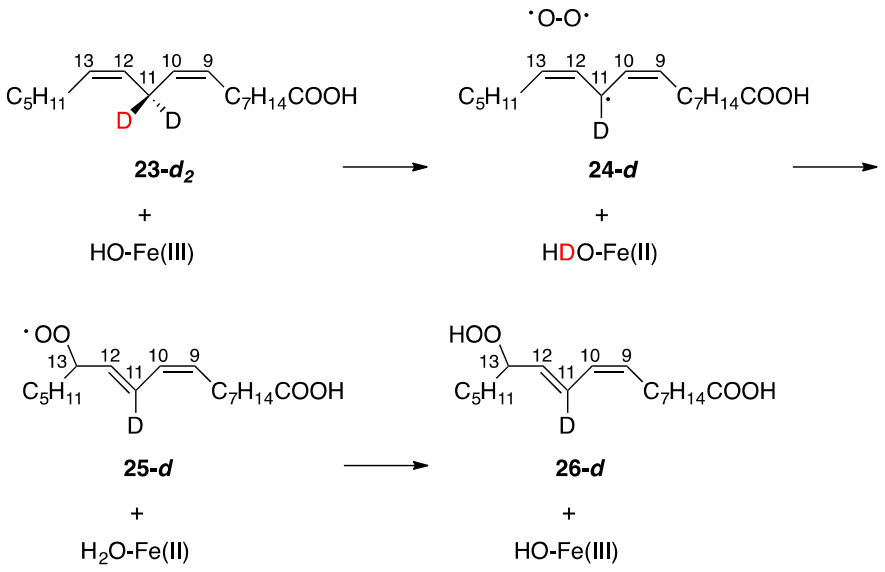

Scheme 7. Linoleic acid oxidation by soybean lipoxygenase 1, where HO-Fe(III) is the catalytic site.

Table 2
Experimental $^{12}C/^{13}C$ KIEs at atoms C9 to C13 for the oxidation of **23-*d*$_2$**

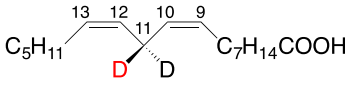

23-*d*$_2$

Atom number	$^{12}C/^{13}C$ KIE[a]
C9	1.025(6)
C10	1.026(9)
C11	1.046(29)
C12	1.035(8)
C13	1.016(4)

[a] Values in parentheses are error bounds in the last two digits.

involvement of C11 in tunneling during abstraction of deuterium in **23-*d*$_2$**.

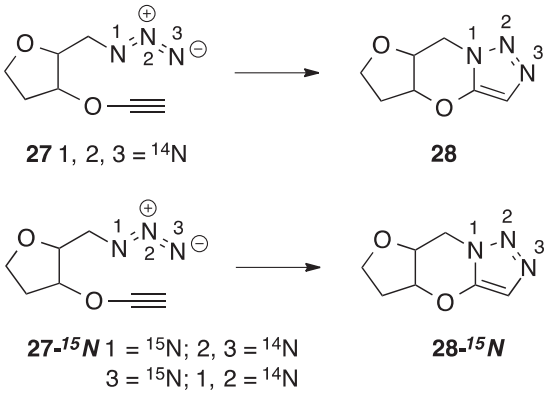

Scheme 8. Intramolecular 'click' reaction of **27**.

4.8. Nitrogen-atom tunneling in a Huisgen reaction

A 2015 computational study describes an intramolecular Huisgen reaction where evidence was found for nitrogen atom tunneling (Scheme 8).[39] Here, a cycloaddition in 2-(azidomethyl)-3-(ethynyloxy)tetrahydrofuran **27** leads to triazole **28**. Computational data included (i) an Arrhenius plot yielded E_a^{CVT}=23.0 kcal/mol, A_{CVT}=2.5×10^{10} s^{-1} whereas $E_a^{CVT+SCT}$=22.5 kcal/mol, $A_{CVT+SCT}$=2.0×10^{10} s^{-1}, at 298 K, which indicated a 35% increase in the reaction rate due to tunneling. Tunneling lowered both the activation energy and the pre-exponential factor due to its barrier width of ~2.4 Å. (ii) Computed $^{14}N/^{15}N$ KIEs (at N1 and at N3) led to KIE_{CVT}=1.01 and $KIE_{CVT+SCT}$=1.04. The $KIE_{CVT+SCT}$ is larger than KIE_{CVT} where values are likely too close to contemplate experiments to distinguish them well.

Heavy atom tunneling is involved in some hydrocarbon and heteroatom reactions, although more publications exist for tunneling of light atoms, as we will see next.

5. Hydrogen atom, hydride, and proton tunneling

We now turn to H•, H$^-$ and H$^+$ organic reactions and discuss examples where tunneling evidence was found. There are 14 literature examples of which 5 contain both experimental *and* theoretical evidence, and 3 literature examples that are based on theoretical evidence alone.

5.1. Hydrogen-atom transfer reactions

5.1.1. 1,3-Hydrogen shift in cyclobutylidenes. A 2014 report describes the hydrogen shift in the conversion of cyclobutylidene **29** and a 3-trimethylsilyl (TMS) **31** derivative to bicyclobutylidenes **30** and **32**, respectively (Scheme 9).[40] Computational data showed the rate of the 1,3-hydrogen migration was enhanced by the TMS group in the γ-position, but that this enhancement was not due to tunneling. On the other hand, rate constants, Arrhenius plots, and KIE data provide evidence for tunneling when comparing **29** and **29-*d***, and when comparing **31** and **31-*d***.

Data were collected and provide evidence of tunneling. (i) Rate constants k_{CVT} and $k_{CVT+SCT}$ were calculated at six temperatures from 77 to 400 K. At 298 K, 73% of the reaction proceeds by tunneling for **29**. At 298 K, 48% proceeds by tunneling for **31**. The contribution of tunneling in **29** is greater than in **31** and effective barrier width of **29** is narrower by 0.1 Å than that **31** making tunneling across a narrower yet larger barrier (E_a^{CVT}=13.7 kcal/mol) in **29** more efficient than through the smaller barrier (E_a^{CVT}=9.5 kcal/mol) in **31**. Furthermore, the contribution of tunneling decreased with an increase in temperature. (ii) Computed Arrhenius plots of

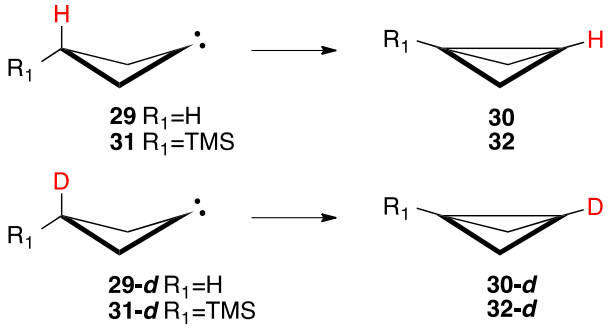

Scheme 9. Hydrogen atom shift in cyclobutylidene and a TMS-substituted cyclobutylidene.

ln $k_{CVT+SCT}$ versus T^{-1} show greater curvature for **29** versus **31**, and greater curvature for **29-*d*** versus **31-*d*** consistent with greater tunneling. The activation energy at 298 K the $E_a^{CVT+SCT}$ was reduced by 1.0 kcal/mol for **29**, and the $E_a^{CVT+SCT}$ was reduced by 0.7 kcal/mol for **31**, when compared to E_a^{CVT} values. (iii) KIEs with inclusion of tunneling ($KIE_{CVT+SCT}=k_H/k_D$) for **31/31-*d*→32/32-*d*** displayed in Table 3 showed a decrease with increasing temperature indicating tunneling.

Table 3
Computed H/D KIEs of **31** without (CVT) and with (CVT+SCT) the inclusion of tunneling

	KIE=k_H(**31**)k_D(**31-*d***)	
T(K)	CVT	CVT+SCT
240	2.29	2.56
300	1.90	2.04
400	1.59	1.63

5.1.2. A 1,3-Hydrogen shift in adamantylidene. A paper appeared in 2014 describing a hydrogen atom shift in the cyclopropanation of adamantylidene **33** to form 2,4-dehydroadamantane **34** (Scheme 10).[41] Here, the H-atom transfer and cyclopropanation occurred in a concerted manner. A singlet diradical was not an actual intermediate; instead, it was located on an inflection point of the potential energy surface reaching **34**.

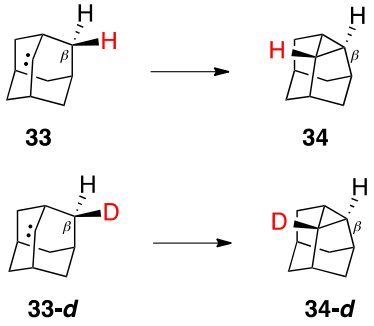

Scheme 10. 1,3-Hydrogen shift in adamantylidene **33**.

B3LYP/6-31G(d,p) calculations also hint at tunneling. At 300 K, the computed rate constants with tunneling of $k_{CVT+SCT}=1.4\times10^5$ s^{-1}, which is approximately twice the k_{CVT} without tunneling implicating that at 300 K this shift occurs mostly by tunneling. H/D KIE was 2.44 below the value of 7 that is more firm evidence of tunneling.

5.1.3. A [1,5]-Sigmatropic shift in cyclopentadienes. An experimental report from 1969[42] and a computational report from 2007[43] have provided evidence for tunneling in the [1,5]-sigmatropic shift of cyclopentadienes (Scheme 11).

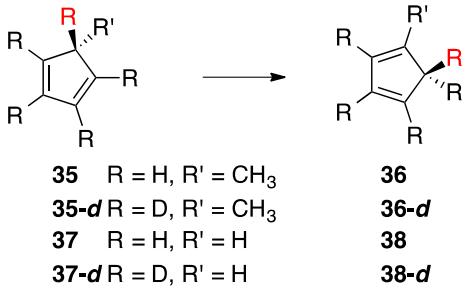

Scheme 11. [1,5]-Sigmatropic shift reactions in cyclopentadienes.

The experimental evidence[42] for tunneling included (i) a temperature dependence in the H/D KIE for **35/35-*d*→36/36-*d***. Measured k_H/k_D for the **35** and **35-*d*** pair were equal to 7.67 at 280 K, 5.75 at 300 K, and 4.70 at 320 K. (ii) A_H/A_D of ~ 0.1 were found, which is less than 1.0 and (iii) $E_a(D)$ - $E_a(H)$ was equal to 2.5 kcal/mol that is >1.2 kcal/mol, and fit within the Kim/Kreevoy criteria as evidence for tunneling.

Computational evidence[43] for tunneling included (i) rate constants k_{CVT} and $k_{CVT+SCT}$ for [1,5]-sigmatropic shifts in **35**, **35-*d***, **37**, and **37-*d*** at 300 K which equated tunneling contributions to 88% for **35**, 73% for **35-*d***, 89% for **37**, and 75% for **37-*d***. (ii) Computed Arrhenius plots of the ln $k_{CVT+SCT}$ versus T^{-1} for the rearrangements of **35** and **37** for 240 K–320 K predicted slight curvature at 240 K–260 K. (iii) Calculations of the H/D KIE for **35** and **37** showed temperature dependence indicative of tunneling. The ratios of $KIE_{CVT+SCT}$ k(**35**)/k(**35-*d***) and k(**37**)/k(**37-*d***) decreased by 60–70 %, from 11.8 to 5.50 and from 11.2 to 5.72, respectively, over range from 280 K to 320 K, which was attributed to a large difference between the activation energies for the shift of hydrogen versus deuterium (e.g., $E_a^{CVT+SCT}$ for the reactions of **35** and **35-*d*** are 4.1 kcal/mol and 1.4 kcal/mol, respectively, while for the reactions of **37** and **37-*d*** are 5.5 kcal/mol and 1.7 kcal/mol, respectively). The data show a modest $KIE_{CVT+SCT}$ (equal to k_H/k_D)=5.50 at room temperature that may hint at tunneling, but does not meet the Kim/Kreevoy criteria of >7. (iv) Differences in activation energies for **35** and **35-*d***, $E_a(D)-E_a(H)=2.5\pm0.3$ kcal/mol is above the Kim/Kreevoy 1.2 threshold to indicate the importance of tunneling.

5.1.4. [1,5]-Sigmatropic shift in pentadienes. Scheme 12 shows the [1,5]-sigmatropic shift of *cis*-1,3-pentadiene **39**.[2,44–48] Computed data[2,44] show a substantial fraction of the hydrogen shift is due to tunneling.

Computational data were collected for isotopomers **39-d_2** and **39-d_3**. (i) $E_a(D)-E_a(H)$ for CVT/SCT compared to CVT is >1.2 kcal/mol, and $A_H/A_D<1.0$ suggesting tunneling (Table 4). (ii) MINDO/3, AM1, and PM3 calculations predicted large KIEs (k_H(**39-d_2**)/k_D(**39-d_3**)) in the [1,5]-sigmatropic shift in pentadiene **39-d_2** and **39-d_3** at temperatures from 463 K to 500 K (Table 5).[46] KIEs without tunneling (KIE_{CVT}) increased 6–7%, while with tunneling ($KIE_{CVT+SCT}$) they increased 18–27% (experimentally it was 13%) over 463 K–500 K.[47] Contribution of tunneling was also corroborated by mPW1K/6-31+G(d,p) KIE calculations for the H-atom transfer in $D_2C{=}CHCH{=}CHCH_3$ **39-d_2** and D-atom transfer in $H_2C{=}CHCH{=}CHCD_3$ **39-d_3** over the temperatures of 400–500 K.[48] The semi-empirical and DFT computed KIEs were lower than experimental values acquired 50 years ago. It is not immediately clear why there is a discrepancy between the computational data and experimental data. However, we note the paper[47] published in 1966 did not assess whether tunneling arose. (iii) The computed transmission coefficients κ_{SCT} provide evidence for the tunneling contribution at

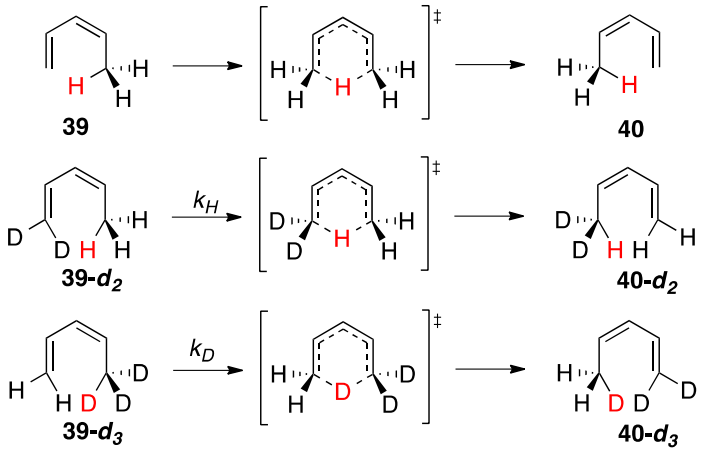

Scheme 12. [1,5]-Sigmatropic shift reactions in pentadiene **39** and isotopomers **39-d_2** and **39-d_3**.

Table 4
Computed pre-exponential factors and Activation energies for **39-d_2** and **39-d_3** without (CVT) and with (CVT+SCT) the inclusion of tunneling

Method	A_H/A_D		$E_a(D)-E_a(H)$ (kcal/mol)	
	CVT	CVT+SCT	CVT	CVT+SCT
MINDO/3	1.1	0.54	0.8	2.0
AM1	1.0	0.24	0.7	2.8
PM3	1.1	0.30	0.9	2.7

Table 5
MINDO/3, AM1 and PM3 computed H/D $KIE_{CVT+SCT}$ for **39-d_2** and **39-d_3**

T(K)	$KIE_{CVT+SCT}=k_H$(**39-d_2**)/k_D(**39-d_3**)		
	MINDO/3	AM1	PM3
463	4.5	5.2	5.7
470	4.3	4.9	5.5
478	4.2	4.7	5.2
500	3.8	4.1	4.6

400 K and 500 K. It was determined that κ_H(**39-d_2**)/κ_D(**39-d_3**) was 2.5 at 400 K and that was 1.5 at 500 K, both of which are greater than 1.0 and indicative of tunneling.[48]

5.1.5. [1,5]-Sigmatropic shift in a diarylpentadiene. Two papers[49,50] reported experimentally derived rate constants for the 1,5-H transfer of (*Z*)-1-*p*-tolyl-5-phenyl-1,3-pentadiene (Scheme 13) at four temperatures spanning 108 K to test for tunneling.

The Arrhenius plot was said to be linear, but no graph was shown[49,50] and the matter was dropped. However, when the data are plotted as seen in Fig. 8, the 4-point linear fit (red dotted line) looks acceptable, but the residuals of the fit are larger than the error bars (numbers in red). This indicates a nonlinear plot; we employed the same procedure as Singleton and Borden[30] to compare slopes in the high versus low temperature regions. The difference in slopes is large, and corresponds to a 4.8 kcal/mol decrease in activation energy. This suggests a significant amount of tunneling, roughly comparable to [1,5]-sigmatropic shift in cyclopentadiene.[43]

5.1.6. [1,7]-Sigmatropic shift in octatrienes. Reports from 1988,[51] 2007[52] and 2014[48] describe the [1,7]-sigmatropic shift of 7-methylocta-1,3,5-triene **43** (Scheme 14).[48,51,52] Experimental and computed work sought evidence for tunneling.

Experimental data included an Arrhenius plot of ln KIE versus T^{-1}, which was curved, but for a few points produced a straight line and a slope $[E_a(D)-E_a(H)]/R$ (where R=gas constant) and intercept A_H/A_D. $E_a(D)-E_a(H)$ was equal to 2 kcal/mol, and A_H/A_D=0.32, both of which point to tunneling by exceeding the Kim/Kreevoy criteria. However, the experimental H/D KIE data were less conclusive for tunneling contributions.[51]

Computational evidence pointed to tunneling including (i) Arrhenius parameters $E_a(D)-E_a(H)$, using CVT with microcanonical optimized multidimensional tunneling corrections μOMT fit better to those obtained experimentally compared to CVT alone.[52] (ii) H/D KIEs were computed including tunneling (by means of CVT+μOMT, squares, Fig. 9) were lower than experimental (solid circles, Fig. 9).[48] When tunneling was accounted for by semiclassical instanton (SI) (solid line, Fig. 9), the H/D KIE of the sigmatropic shift were in even better agreement with experimental results.[48] Similar to [1,5]-sigmatropic shifts in Section 5.1.4, here the computational data were fair in reproducing the experimental data.

5.1.7. Hydrogen-atom transfer in tetralin autoxidation. In 2015, a report appeared with experimental H/D KIE evidence of hydrogen atom tunneling from tetralin (**45-d_2**, Scheme 15) or diethylbenzene, or dibenzylbenzene to a peroxyl radical.[53] These experiments were carried out at 65 °C. The KIE for formation of products **47-d_2** and **49-*d*** was found to be 15.9±1.4, which exceeded the Kim/Kreevoy criterion ~7, suggesting significant contribution of tunneling in the H abstraction. Similar effects were observed for diethylbenzene and dibenzylbenzene for conversion to hydroperoxide. The KIE of diethylbenzene was measured to be 13.7±2.0, and that of dibenzylbenzene was measured to be 12±2.0.

5.1.8. Double-hydrogen atom transfer in solid-state porphycenes. A 2016 report described hydrogen atom tunneling in the tautomerization of porphycenes **50** and **51** (Scheme 16).[54] These

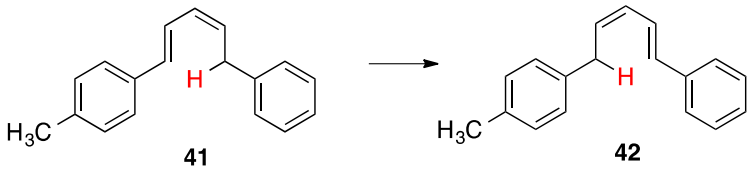

Scheme 13. [1,5]-Sigmatropic shift in (*Z*)-1-*p*-tolyl-5-phenyl-1,3-pentadiene **41**.

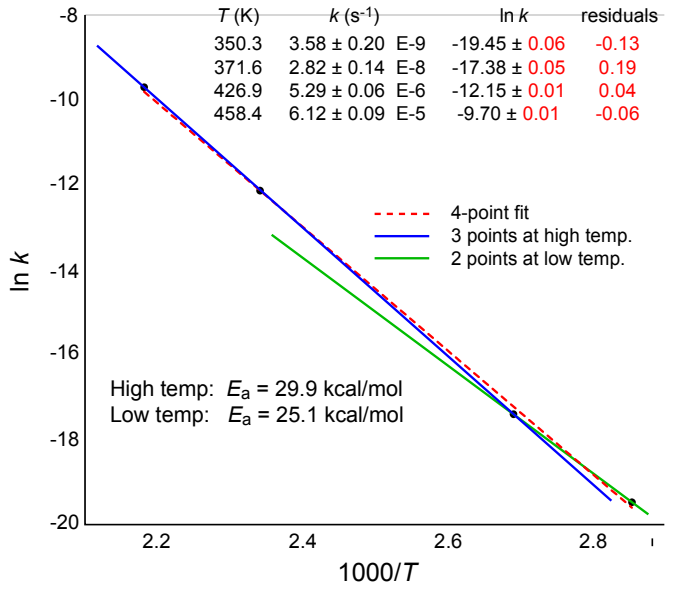

Fig. 8. Arrhenius plot for the [1,5]-sigmatropic shift reaction in pentadiene **41** in Scheme 13. The residuals of the linear fit are larger than the error bars (shown in red), which show the plot is nonlinear. Separate lines at low and high temperature give a difference in E_a of 4.8 kcal/mol. The significant curvature at low temperature suggests that tunneling is important in this reaction.

tautomerizations occur by a double hydrogen atom transfer in both the ground and excited states of the porphycenes.

Experimental evidence for tunneling included (i) Arrhenius plots of the ground-state (S_0) and excited-state (S_1) hydrogen transfer rate constant ln k vs T^{-1} for the temperature range of 20 K–400 K were plotted for **50**, **51**, **50-*d*$_2$**, and **51-*d*$_2$** and showed curvature. Arrhenius plots for **50-*d*$_2$** and **51-*d*$_2$** showed less tunneling than for **50** and **51** due the greater mass of deuterium. (ii) H/D KIEs (for k_{HH}/k_{DD}) were measured for ground-state tautomerization in **50** and **51** were >7 and revealed tunneling for **50** at T<270 K and for **51** at T<370 K. Themes on hydrogen atom transfer in organometallic chemistry have been reported, as we will see next.

5.1.9. Hydrogen-atom transfer from hydrocarbon to an osmium-centered radical. A 2014 paper reported on the homolysis of bilaterally symmetrical compounds $[Cp(CO)_2Os]_2$ and $[\eta^5\text{-}^i Pr_4C_5H(CO)_2Os]_2$ (Scheme 17).[55] Here, osmium radicals $Cp(CO)_2Os^\bullet$ **52** and $\eta^5\text{-}^i Pr_4C_5H(CO)_2Os^\bullet$ **54** were shown to have utility in tunneling with hydrogen atom donors fluorene, xanthene, 9,10-dihydroanthracene, and 1,4-cyclohexadiene.

Experimental evidence for tunneling included (i) activation parameters for H donation from xanthene to $\eta^5\text{-}^i Pr_4C_5H(CO)_2Os^\bullet$ was $E_a(D)-E_a(H)=3.3\pm0.2$ kcal/mol^{-1} and $A_H/A_D=0.06\pm0.02$ [Kim/Kreevoy criteria are $E_a(D)-E_a(H)$ are greater than ~1.2 kcal/mol and A_H/A_D is less than 1.0]. (ii) H/D KIEs were determined using time resolved IR and ^{1}H NMR spectroscopy and ranged from 9.3 to 16.8 at 25 °C, where

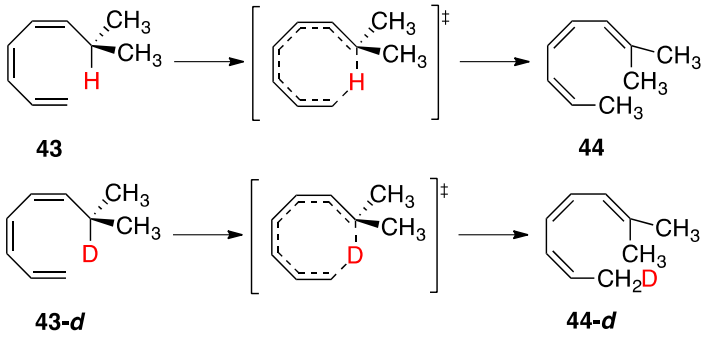

Scheme 14. The [1,7]-sigmatropic shift in octa-1,3,5-triene **43** to form octa-2,4,6-triene **44**.

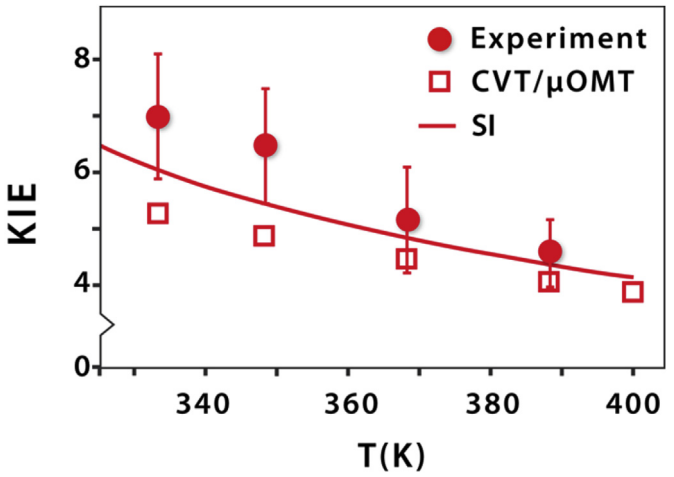

Fig. 9. KIE for the [1,7]-sigmatropic shift of octa-1,3,5-triene **43**. The solid circles are the experimental data, the solid line is the mPWB1K/6-31G+(d,p) with semiclassical instanton, the open squares are the PES from mPWB1K/6-31+G(d,p), and the dashed line is the classical transition state theory. The calculations were without (CVT) and with (CVT+μOMT) the inclusion of tunneling. Adapted with permission from ref 48. Copyright 2014 American Chemical Society.

Kim/Kreevoy criteria for H/D KIE is above ~7. The H/D KIEs from 10 °C to 70 °C for $\eta^5\text{-}^i Pr_4C_5H(CO)_2Os^\bullet$ with xanthene and fluorine showed a temperature dependence. The results reveal H/D KIEs of 6.2 (70 °C) to 17.9 (10 °C) for xanthene, and 9.8 (70 °C) and 18.0 (10 °C) for fluorene with $Cp(CO)_2Os^\bullet$, $\eta^5\text{-}^i Pr_4C_5H(CO)_2Os^\bullet$, respectively.

5.1.10. Release of methane from hydridomethylbis-phosphine platinum complexes. An experimental report from 1978[56] described primary H/D KIEs of methylbis(triphenylphosphine) platinum **56** and **56-*d***for the reductive elimination of methane (Scheme 18). The H/D KIE of k(**56**)/k(**56-*d***) was equal to 3.3±0.3 at 248K,[56] which is a modest value and thus involvement of tunneling could not be concluded with any certainty. Recently, a computational report from 2008[57] describes a reductive elimination of methane and elaborates on possible tunneling contributions.

Computational evidence for tunneling included (i) the rate constant at 248 K for **57** without tunneling is $k_{CVT}=1.27\times10^{-4}$ s^{-1} and with tunneling is $k_{CVT+SCT}=5.11\times10^{-4}$ s^{-1}, where the latter rate constant is in a better agreement with the experimental value of $k=(4.5\pm0.5)\times10^{-4}$ s^{-1} for **56**. Thus at 248 K, 86% of the reductive elimination of methane from **57** is attributed to involve tunneling, and lower the E_a by 1.7 kcal/mol. Primary KIEs for reductive elimination of methane (data not shown) were inconclusive to deduce

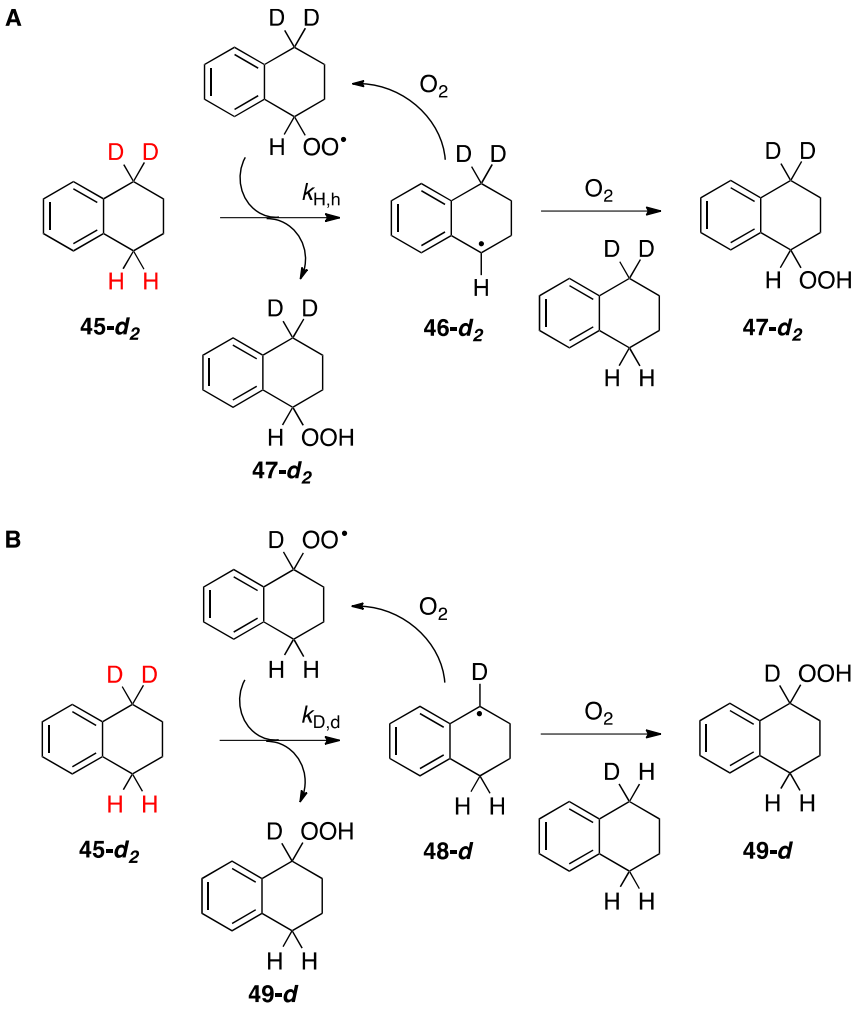

Scheme 15. Autoxidation reactions of tetralin **45-*d*$_2$**.

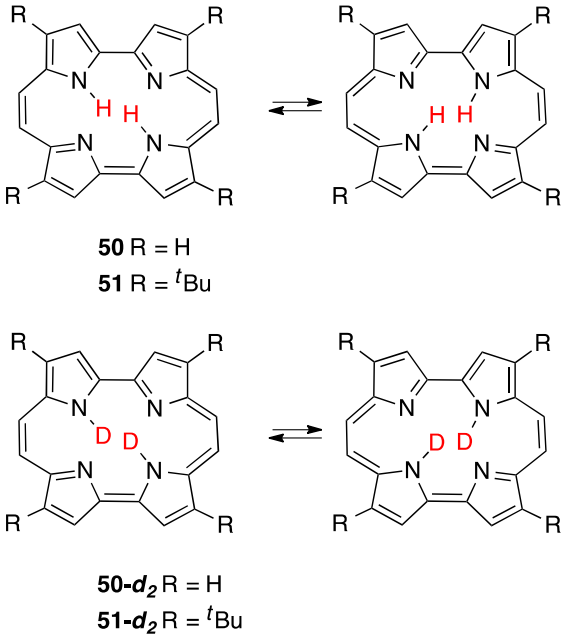

Scheme 16. Tautomerizations of porphycenes **50** and **51**.

tunneling contributions, thus secondary KIEs were sought. (ii) Secondary KIEs were computed for *k*(**57**)/*k*(**58-*d*$_3$**), and compared to *k*(**57-*d***)/*k*(**58-*d*$_4$**). Based on CVT, calculations without tunneling *k*(**57**)/*k*(**58-*d*$_3$**)=0.99 and *k*(**57-*d***)/*k*(**58-*d*$_4$**)=1.00, whereas inclusion of tunneling CVT+SCT show a relative difference between secondary KIEs with *k*(**57**)/*k*(**58-*d*$_3$**)=1.35 and *k*(**57-*d***)/*k*(**58-*d*$_4$**)=1.06.

5.1.11. C–H amination involving iron imido complexes. An intriguing report from 2011 describes the C–H amination of high-spin iron imido complexes **59** and **60** (Scheme 19).[58] Here, this is an example where tunneling contributes in conjunction with catalysis. Experimental evidence for tunneling included a large H/D KIE of 12.8 for the reaction of (^{Ad}L)Fe^{II}Cl(OEt$_2$) **59**, azidoadamantane and toluene at 60 °C (Scheme 19A). An even larger H/D KIE of 24 was observed for the reaction of (^{Ar}L)FeCl(NC$_6$H$_4$-*p*-^{t}Bu) **60** at room temperature (Scheme 19B). Both values for H/D KIE are above 7 and far exceed Kim/Kreevoy criteria.

5.2. Hydride shift reactions

5.2.1. Hydride shift from an NADH analogue to a dioxoruthenium(VI) complex. In 2015, a report appeared on *trans*-[Ru^{VI}(TMC)(O)$_2$]$^{2+}$ (TMC=1,4,8,11-tetramethyl-1,4,8,11-tetraazacyclotetradecane) **61** that received a hydride from an NADH analogue, 10-methyl-9,10-dihydroacridine (AcrH$_2$) **62** (Scheme 20).[59] By monitoring the UV

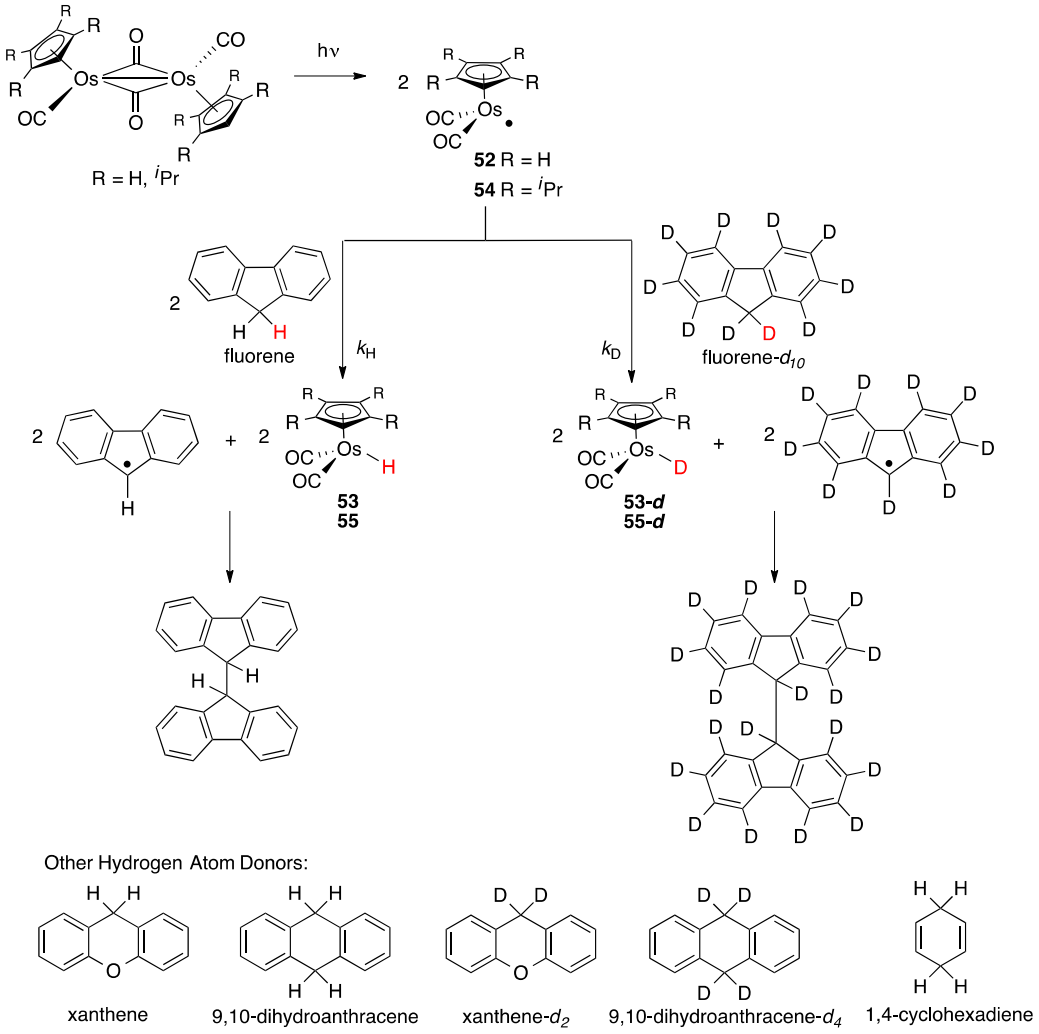

Scheme 17. Hydrogen atom transfer between hydrocarbons and osmium-centered radicals **52** and **54**.

band appearance at 358 nm (ε=1.8×10^4 M^{-1} cm^{-1}), experimental evidence for hydride tunneling included large H/D KIE of 13 in acetonitrile at 0 °C. Again, this large H/D KIE is above the Kim/Kreevoy criteria.

5.2.2. Hydride shift of glyceraldehyde to dihydroxyacetone. In 2015 a report described a hydride shift in the isomerization of glyceraldehyde **65** to dihydroxyacetone **69** (Scheme 21).[60] Dehydration of triol **65** and Ca^{2+} complexation led to **67**, where experimental and computational data provided evidence for the tunneling in the hydride shift step of **67** to **68**.

Experimental evidence for hydride tunneling included (i) rates at which 2-protioglyceraldehyde **66** and 2-deuteroglyceraldehyde **66-*d*** converted to dihydroxyacetone **69** and **69-*d***, respectively show E_a(H)=8.5 kcal/mol and E_a(D)=10.6 kcal/mol where E_a(D)–E_a(H) >2.2 kcal/mol (ii) The experimental pre-exponential factors were A_H=97.9 and A_D=344.2 and yielded A_H/A_D=0.28. (iii) The H/D KIEs were found to be large, that is 14.9, 9.3 and 5.1 at temperatures of 0 °C, 40 °C, and 80 °C. The above results for (i)-(iii) fit the Kim/Kreevoy criteria.

Computational evidence was collected for tunneling. B3LYP/6-31++G(d,p) calculations were used with POLYRATE and polarized continuum model water solvation, and a single point CCSD(T)/6-31++G(d,p) energy correction for conversion of **67** to **68**. The predicted Arrhenius parameters also exceeded Kim/Kreevoy criteria, in which the E_a(H)=17.8 kcal/mol and E_a(D)=19.3 kcal/mol, thus giving E_a(D) - E_a(H)=1.5 kcal/mol, and A_H/A_D=0.43. The computed KIEs by CVT+SCT for the Arrhenius plot of ln KIE versus T^{-1} over the range of 0–80 °C were in reasonable agreement with the experiments. Based on the calculations, at least 56–80% of the reaction proceeds by tunneling at 0–80 °C.

5.3. Proton transfer reactions

Some equilibrium reactions take place and indicate that tunneling is not always a one-way street. There have been reports of proton tunneling that are in tautomerization reactions.

5.3.1. Tautomerization of thiotropolone. In 2011[61] and 2012,[62] reports appeared with evidence for tunneling in thiotropolone tautomers **70** and **71** (Scheme 22). Experimental ^{13}C and ^{17}O NMR spectroscopy indicated the existence of **70**:**71** in ratio of 58:42 that did not change over a temperature range (−130 °C and 27 °C), as well as in the molten state (at 60 °C).[61]

Computational studies added further evidence of tunneling, including (i) MPW1K and MP2 calculations of **70** for proton transfer over the temperature range −130 °C to 60 °C show k_{CVT} increased

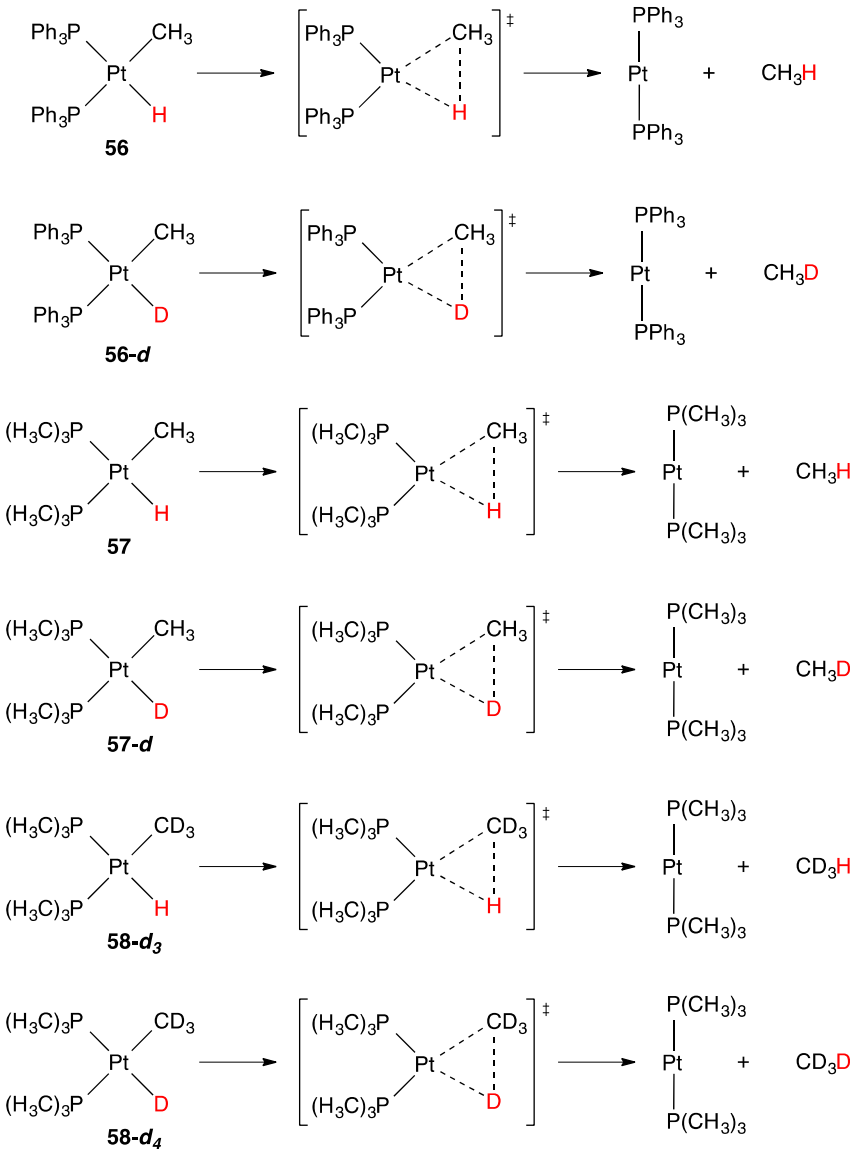

Scheme 18. Reductive elimination of methane from methylbis-phosphine platinum complexes.

by $\sim 10^5$, but $k_{CVT+SCT}$ only increased 1.6 times indicating near invariance to temperature.[62] (ii) The Arrhenius plot for the ln $k_{CVT+SCT}$ versus T^{-1} of **70**⇌**71** show a large tunneling contribution over wide temperature range. (iii) Computed values of H/D $KIE_{CVT+SCT}$ for **70** and **70-*d*** were large, Table 6, which are greater than Kim/Kreevoy criteria of H/D KIE of >7. (iv) Without tunneling the E_a^{CVT} was 5.8 kcal/mol, and log A_{CVT}=11.9 s^{-1}, and with the SCT tunneling correction the $E_a^{CVT+SCT}$=0.3 kcal/mol and log $A_{CVT+SCT}$=1.3 s^{-1}, indicating that tunneling decreases the energy of activation. Computations showed that the barrier is narrow so that 97% of the thiotropolone reaction is due to proton tunneling in molten state at 60 °C.

Other than thiotropolones, tropolones contain tautomers that interconvert with a tunneling contribution. Computational methods show that 75% of the tropolone reaction is due to proton tunneling.[62]

5.3.2. Tautomerism of an aminofulvene-aldimine. A 2008 report describes the tautomerization of *N,N′*-diphenyl-6-aminofuvene-1-aldimine **72**, in which the proton transfer of N–H···N to N···H–N is an ultrafast process (Scheme 23).[63] Fig. 10 shows an Arrhenius plot for the H (○) and D (■) transfer process in crystalline and amorphous phases. The tautomerism is faster in the amorphous phase than the crystalline phase, in which curvature in both phases was interpreted as evidence of tunneling. The H/D KIE for the amorphous phase was 4 and for the crystalline phase was 9 suggesting tunneling contributions in both.

6. Summary

Tunneling contributes, to varying extents, in organic reactions. Sections 4 and 5 described the tunneling of heavy and light atoms, respectively. Fewer publications exist for heavy atom tunneling (Section 4) than light atom tunneling (Section 5), but this does not mean the former is less important. Evidence suggests nontrivial percentages for heavy atom tunneling in a Roush allylboration (36%), a Au(III) promoted C–C bond formation (28%), an azide cycloaddition (35%), and a Bergman cyclization (39%), which can occur at temperatures from −78 °C to 37 °C. Literature examples sometimes point to high percentages of light atom tunneling, e.g., in cyclobutylidene

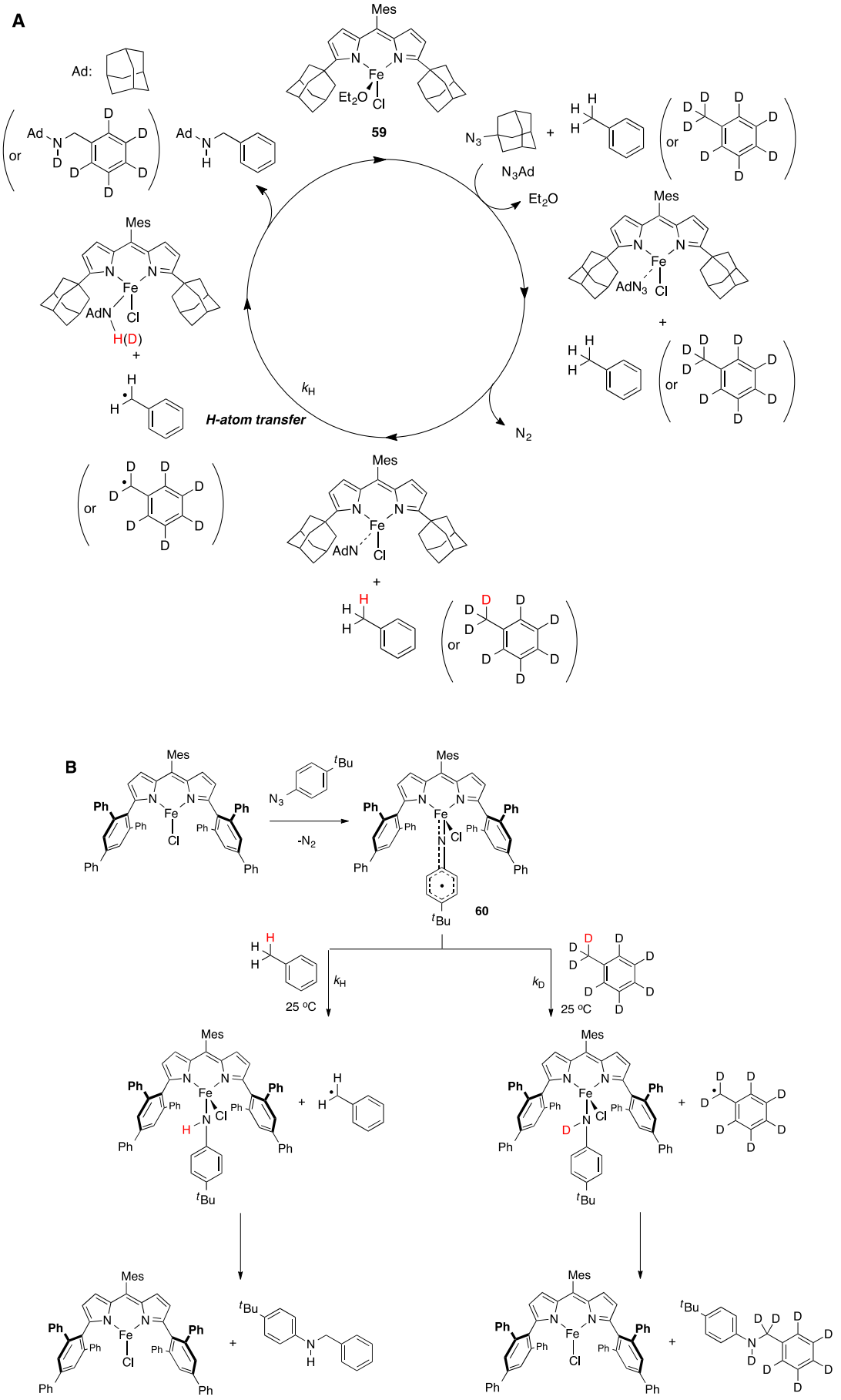

Scheme 19. Proposed mechanisms of C–H amination involving adamantane iron imido complex **59** (**A**) and iron imido complex **60** (**B**).

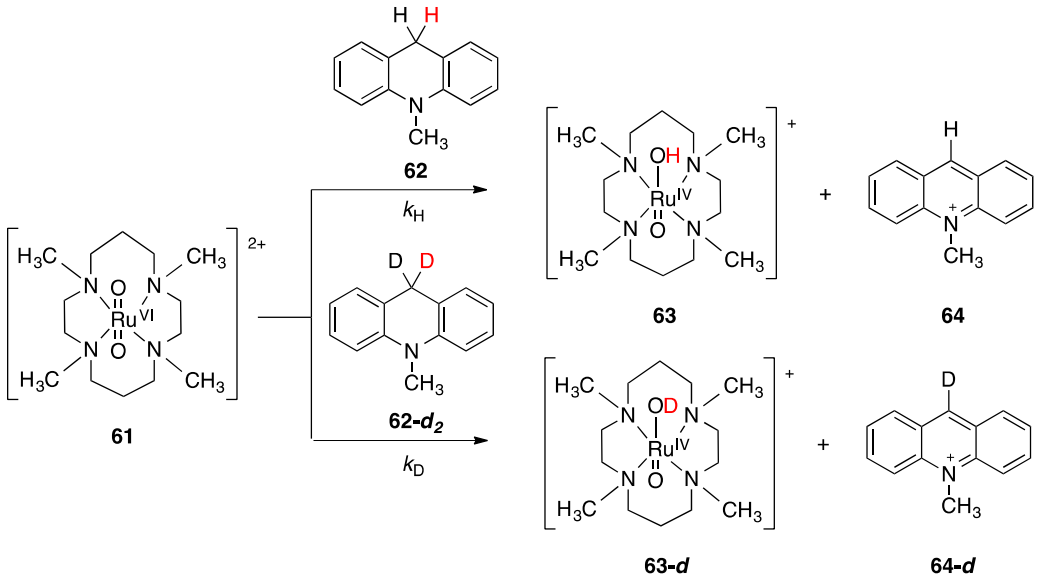

Scheme 20. Intermolecular hydride shift from NADH analogue **62** to dioxoruthenium(VI) complex **61**.

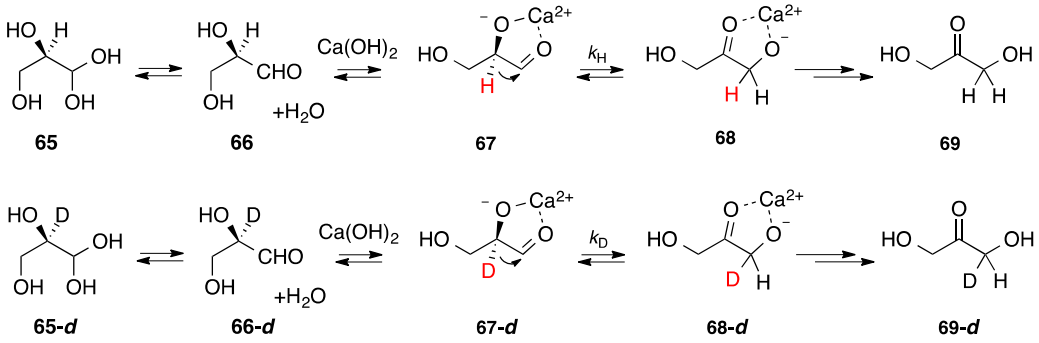

Scheme 21. Isomerization of glyceraldehyde **66** to dihydroxyacetone **69** by a hydride shift.

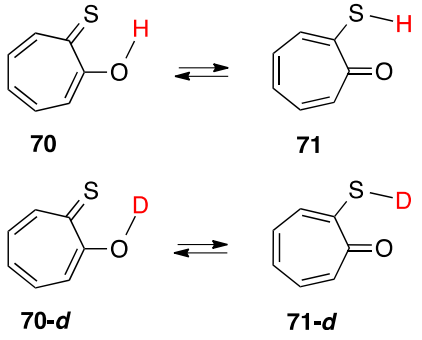

Scheme 22. Intramolecular H and D transfer of thiotropolone **70** and **70-*d***.

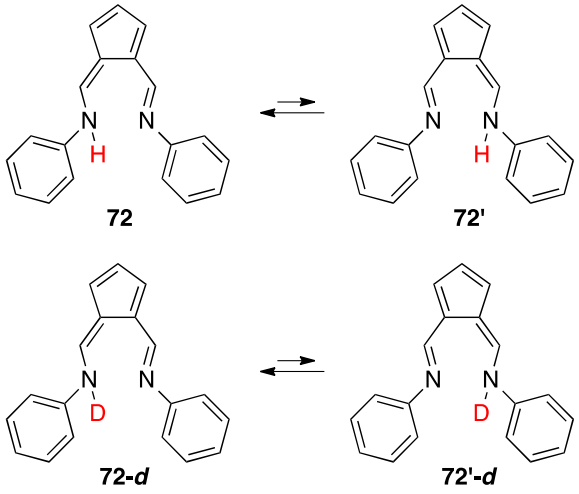

Scheme 23. Tautomerization of aminofulvene-aldimine **72**. Tautomers **72′** and **72′-*d*** are not degenerate with **72** and **72-*d***, respectively, due to intermolecular interaction in the solid state.

Table 6
Computed H/D $KIE_{CVT+SCT}$ for **70** and **70-*d***

T(°C)	$KIE_{CVT+SCT}=k_H$(**70**)/k_D(**70-d**)
−130	1.22×103
−100	1.11×103
−60	1.01×103
25	9.22×102
60	8.53×102

(73%), in dihydroxyacetone (56–80%), and in thiotropolone (60–97%), which can occur at temperatures from 0 °C to 80 °C.

What are the future prospects of tunneling in organic chemistry? The future looks promising although more facile methods are needed to detect tunneling. Experimentally, detection of carbon-atom tunneling

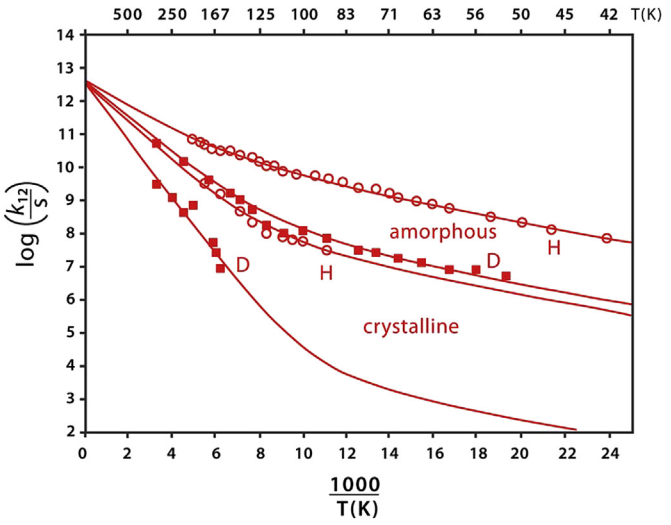

Fig. 10. Arrhenius plot for H/D transfer from the rate constants in **72**. Lines were generated by fitting data to the Bell-Limbach tunneling model. Adapted with permission from ref 63. Copyright 2008 American Chemical Society.

can be difficult due to low ^{13}C natural abundance, although reactions on larger scales is one solution to this problem.[64] Furthermore, theoretical methods that map discontinuous potential energy surfaces can run into difficulty in screening for tunneling. Nevertheless, computational methods can deduce tunneling contributions by calculating small-curvature tunneling (SCT) and canonical variational transition state theory (CVT) and thus ferret out classical contributions to the rate. Tunneling has a desired caveat of increasing the speed to reach product through the barrier instead of over the barrier. Lastly, *tunneling control*[5,65,66] provides an additional mechanistic tool along with conventional kinetic and thermodynamic control.

Acknowledgements

E.M.G. and K.K. acknowledge support from the donors of the Petroleum Research Fund of the American Chemical Society and PSC-CUNY. E.M.G. also acknowledges the Eugene Lang Foundation at Baruch College. The National Science Foundation is acknowledged for the support of A.G. (CHE-1464975) and C.D. (CHE-1465040). We thank Leda Lee for the graphic arts work and discussions.

References and notes

1. Bell, R. P. In *The Tunnel Effect in Chemistry*; Chapman and Hall: 1980; pp 12–175.
2. Dewar, M. J. S.; Merz, K. M., Jr.; Stewart, J. J. P. *Chem. Commun.* **1985**, 166–168.
3. Meisner, J.; Kästner, J. *Angew. Chem., Int. Ed. Engl.* **2016**, *55*, 2–16.
4. Borden, T. W. *WIREs Comput. Mol. Sci.* **2016**, *6*, 20–46.
5. Ley, D.; Gerbig, D.; Schreiner, P. R. *Org. Biomol. Chem.* **2012**, *10*, 3781–3790.
6. Kästner, J. *WIREs Comput. Mol. Sci.* **2014**, *4*, 158–168.
7. Pu, J.; Gao, J.; Truhlar, D. G. *Chem. Rev.* **2006**, *106*, 3140–3169.
8. Fernandez-Ramos, A. J.; Miller, A.; Klippenstein, S. J.; Truhlar, D. G. *Chem. Rev.* **2006**, *106*, 4518–4584.
9. Hiraoka, K. In *Atom Tunneling Phenomena in Physics, Chemistry and Biology*; Miyazaki, T., Ed.; Springer: Berlin, Germany, 2004; pp 173–199.
10. Johannissen, L. O.; Haya, S.; Scrutton, N. S. *Phys. Chem. Chem. Phys.* **2015**, *17*, 30775–30782.
11. Layfield, J. P.; Hammes-Schiffer, S. *Chem. Rev.* **2014**, *114*, 3466–3494.
12. Nagel, Z. D.; Klinman, J. P. *Chem. Rev.* **2010**, *110*, PR41–PR67.
13. Dybala-Defratyka, A.; Paneth, P.; Truhlar, D. G. In *Quantum Tunnelling in Enzyme-catalyzed Reactions*; Allemann, R. K., Scrutton, N. S., Eds.; RSC Cambridge: 2009; pp 36–78.
14. Nagel, Z. D.; Klinman, J. P. *Chem. Rev.* **2006**, *106*, 3095–3118.
15. Kohen, A. In *Isotope Effects in Chemistry and Biology*; Kohen, A., Limbach, H. H., Eds.; Taylor and Francis: Boca Raton, FL, 2006; pp 744–758.
16. Kohen, A. *Prog. React. Kinet. Mech.* **2003**, *28*, 119–156.
17. Bruno, W. J.; Bialek, W. *Biophys. J.* **1992**, *63*, 689–699.
18. Karmakar, S.; Jose, D.; Datta, A. *Reson.* **2014**, 160–174.
19. Sheridan, R. S. In *Reactive Intermediate Chemistry*; Moss, R. A., Platz, M. S., Jones, M., Jr., Eds.; John Wiley & Sons: New York, NY, 2007; pp 415–463.
20. Goldanskii, V. I. *Annu. Rev. Phys. Chem.* **1976**, *27*, 85–126.
21. Zheng, J.; Zhang, S.; Lynch, B. J.; Corchado, J. C.; Chuang, Y.-Y.; Fast, P. L.; Hu, W.-P.; Liu, Y.-P.; Lynch, G. C.; Nguyen, K. A.; Jackels, C. F.; Fernandez Ramos, A.; Ellingson, B. A.; Melissas, V. S.; Villà, J.; Rossi, I.; Coitiño, E. L.; Pu, J.; Albu, T. V. *POLYRATE—version 2010A*; University of Minnesota: Minneapolis, MN, 2010.
22. Truhlar, D. G.; Garrett, B. C. *J. Phys. Chem. A* **2003**, *107*, 4006–4007.
23. Fernandez-Ramos, A.; Ellingson, B. A.; Garrett, B. C.; Truhlar, D. G. In *Reviews in Computational Chemistry*; Lipkowitz, K. B., Cundari, T. R., Eds.; Wiley: Hoboken, NJ, 2007; pp 584–619.
24. Skodje, R. T.; Truhlar, D. G.; Garrett, B. C. *J. Phys. Chem.* **1981**, *85*, 3019–3023.
25. Truhlar, D. G.; Garrett, B. C. *Annu. Rev. Phys. Chem.* **1984**, *35*, 159–189.
26. Garrett, B. C.; Truhlar, D. G. *J. Phys. Chem.* **1979**, *83*, 2921–2926.
27. Anslyn, E. V.; Dougherty, D. A. *Modern Physical Organic Chemistry*; University Science Books, 2006; pp 435–437.
28. Bell, R. P. *Proc. R. Soc. Lond. A* **1935**, *148*, 241–250.
29. Kim, Y.; Kreevoy, M. M. *J. Am. Chem. Soc.* **1992**, *114*, 7116–7123.
30. Gonzalez-James, O. M.; Zhang, X.; Datta, A.; Hrovat, D. A.; Borden, W. T.; Singleton, D. A. *J. Am. Chem. Soc.* **2010**, *132*, 12548–12649.
31. Vetticatt, M. J.; Singleton, D. A. *Org. Lett.* **2012**, *14*, 2370–2373.
32. Greer, E. M.; Cosgriff, C. V.; Doubleday, C. *J. Am. Chem. Soc.* **2013**, *135*, 10194–10197.
33. Karmakar, S.; Datta, A. *J. Phys. Chem. B* **2016**, *120*, 945–950.
34. Carpenter, B. K. *J. Am. Chem. Soc.* **1983**, *105*, 1700–1701.
35. Kozuch, S. *RSC Adv.* **2014**, *4*, 21650–21656.
36. Wolf, J. W.; Winston, M. S.; Toste, F. D. *Nat. Chem.* **2014**, *6*, 159–164.
37. Nijamudheen, A.; Karmakar, S.; Datta, A. *Chem.—Eur. J.* **2014**, *20*, 14650–14658.
38. Meyer, M. P.; Klinman, J. P. *J. Am. Chem. Soc.* **2011**, *133*, 430–439.
39. Karmakar, S.; Datta, A. *J. Phys. Chem. B* **2015**, *119*, 11540–11547.
40. Karmakar, S.; Datta, A. *J. Phys. Chem. B* **2014**, *118*, 2553–2558.
41. Kozuch, S. *Phys. Chem. Chem. Phys.* **2014**, *16*, 7718–7727.
42. McLean, S.; Webster, C. J.; Rutherford, R. D. J. *Can. J. Chem.* **1969**, *47*, 1555–1559.
43. Shelton, G. R.; Hrovat, D. A.; Borden, W. T. *J. Am. Chem. Soc.* **2007**, *108*, 3253–3258.
44. Dormans, G. J. M.; Buck, H. M. *J. Am. Chem. Soc.* **1986**, *129*, 164–168.
45. Chantranupong, L.; Wildman, T. A. *J. Am. Chem. Soc.* **1990**, *112*, 4151–4154.
46. Liu, Y.-P.; Lynch, G. C.; Truong, T. N.; Lu, D. H.; Truhlar, D. G.; Garett, B. C. *J. Am. Chem. Soc.* **1993**, *115*, 2408–2415.
47. Roth, W. R.; König, J. *Liebigs Ann. Chem.* **1966**, *699*, 24–32.
48. Kryvohuz, M. *J. Phys. Chem. A* **2014**, *118*, 535–544.
49. Doering, W. von E.; Keliher, E. J.; Zhao, X. *J. Am. Chem. Soc.* **2004**, *126*, 14206–14216.
50. Doering, W. von E.; Zhao, X. *J. Am. Chem. Soc.* **2006**, *128*, 9080–9085.
51. Baldwin, J. E.; Reddy, P. *J. Am. Chem. Soc.* **1988**, *110*, 8223–8228.
52. Mousavipour, S. H.; Fernández-Ramos, A.; Meana-Pañeda, R.; Martínez-Núñez, E.; Vázquez, S. A.; Ríos, M. A. *J. Phys. Chem. A* **2007**, *111*, 719–725.
53. Muchalski, H.; Levonyak, A. J.; Xu, L.; Ingold, K. U.; Porter, N. A. *J. Am. Chem. Soc.* **2015**, *137*, 94–97.
54. Ciaćka, P.; Fita, P.; Listkowski, A.; Radzewicz, C.; Waluk, J. *J. Phys. Chem. Lett.* **2016**, *7*, 283–288 Waluk, *J. Chem. Rev.* **2016** (in press) (DOI: 10.1021/acs.chemrev.6b00328).
55. Lewandowska-Andralojc, A.; Grills, D. C.; Zhang, J.; Bullock, R. M.; Miyazawa, A.; Kawanishi, Y.; Fujita, E. *J. Am. Chem. Soc.* **2014**, *136*, 3572–3578.
56. Abis, L.; Sen, A.; Halpern, J. *J. Am. Chem. Soc.* **1978**, *100*, 2915–2916.
57. Datta, A.; Hrovat, D. A.; Borden, W. T. *J. Am. Chem. Soc.* **2008**, *130*, 2726–2727.
58. King, E. R.; Hennessy, E. T.; Betley, T. A. *J. Am. Chem. Soc.* **2011**, *133*, 4917–4923.
59. Dhuri, S. N.; Lee, Y. M.; Seo, M. S.; Cho, J.; Narulkar, D. D.; Fukuzumi, S.; Nam, W. *Dalton Trans.* **2015**, *44*, 7634–7642.
60. Cheng, L.; Doubleday, C.; Breslow, R. *Proc. Natl. Acad. Sci. U.S.A.* **2015**, *112*, 4218–4220.
61. Machiguchi, T.; Hasegawa, T.; Saitoh, H.; Yamabe, S.; Yamazaki, S. *J. Org. Chem.* **2011**, *76*, 5457–5460.
62. Jose, D.; Datta, A. *Angew. Chem., Int. Ed. Engl.* **2012**, *51*, 9389–9392.
63. Lopez del Amo, J. M.; Langer, U.; Torres, V.; Buntkowsky, G.; Vieth, H.-M.; Pérez-Torralba, M.; Sanz, D.; Claramunt, R. M.; Elguero, J.; Limbach, H.-H. *J. Am. Chem. Soc.* **2008**, *130*, 8620–8632.
64. Singleton, D. A.; Thomas, A. A. *J. Am. Chem. Soc.* **1995**, *117*, 9357–9358.
65. Schreiner, P. R.; Reisenauer, H. P.; Ley, D.; Gerbig, D.; Wu, C.-H.; Allen, W. D. *Science* **2011**, *332*, 1300–1303.
66. Ley, D.; Gerbig, D.; Schreiner, P. R. *Chem. Sci.* **2013**, *4*, 677–684.

Biographical sketches

Edyta M. Greer received her M.S. degree at the University of Warsaw and her Ph.D. in physical organic chemistry at the Graduate Center of the City University of New York (CUNY). After postdoctoral work at Cornell University with Roald Hoffmann, she joined the faculty at the Baruch College of CUNY in 2008 and is currently an associate professor. Her research uses computational chemistry to study planar chirality, isotope effects, tunneling and diradicals.

Alexander Greer is a professor at Brooklyn College of CUNY. He received his Ph.D. from the University of Wyoming with Edward Clennan, and was a postdoctoral fellow at the UCLA with Christopher Foote. He has co-founded the company Singlet O_2 Therapeutics LLC. His research interests are in oxidation reactions, photochemistry, and devices for photodynamic therapy.

Kitae Kwon was born in Seoul, South Korea. He joined the laboratory of Prof. Edyta Greer and obtained his B.A. degree in Chemical Biology with a minor in French at Baruch College of CUNY. His research interests thus far are in theoretical organic chemistry. He is the recipient of awards including the CUNY Nobel Prize Challenge and an ACS Travel Grant for undergraduates.

Charles Doubleday received his undergraduate degree at the University of Kansas and his Ph.D. at the University of Chicago with Gerhard Closs. At Columbia University, he teaches organic chemistry and his research interests are in the area of computational dynamics of chemical reactions and reactive intermediates, and quantum mechanical tunneling.